Available online at www.sciencedirect.com
SCIENCE DIRECT®
Journal of Magnetic Resonance 175 (2005) 30–43
JMR Journal of Magnetic Resonance
www.elsevier.com/locate/jmr

Spin-echo MRS in humans at high field: LASER localisation using FOCI pulses

Paul Kinchesh *, Roger J. Ordidge

Department of Medical Physics and Bioengineering, University College London, Wellcome Trust High Field MR Research Laboratory, 12 Queen Square, London WC1N 3AR, UK

Received 25 August 2004; revised 23 February 2005
Available online 14 April 2005

Abstract

Significant improvements in spin-echo MRS are possible when voxel localisation is performed using high bandwidth frequency offset corrected inversion (FOCI) pulses as opposed to more conventional lower bandwidth pulses. The reduced chemical shift displacement errors result in a spectrum that more accurately reflects the actual metabolite distribution within any region of interest that is selected graphically on a series of scout images, and can lead to improved metabolite detection in the case of homonuclear *J*-coupled spins. At 4.7 T, FOCI pulses with a 20 kHz bandwidth result in extremely sharp and uniform selection profiles, and negligible contamination from outside of the voxel of interest, for all signals in the ^{1}H spectral range that is normally studied. A 'FOCI' adiabatic half-passage is observed to provide good excitation over the ^{1}H spectral range. Single shot performance with echo-time (TE) $\geqslant$ 48 ms is reported using a four-port drive birdcage head coil. GAMMA simulations show that, for many detectable metabolites at 4.7 T, LASER localisation using FOCI pulses with TE = 48 ms results in ^{1}H anti-phase spectral components that are the same order as would be obtained from a symmetric PRESS sequence with TE = 32 ms. Timing schemes are proposed to enable good measurement of lactate with very little signal loss arising from chemical shift displacement errors at TE = 144 and 288 ms.

Keywords: Spin-echo; MRS; LASER; Localisation; FOCI pulses

1. Introduction

Localised in vivo NMR spectroscopy (MRS) is a useful tool for studying numerous disease states in humans. In particular, the direct and detailed information provided by MRS at a biochemical level can augment understanding of the underlying mechanisms involved. Furthermore, MRS is often able to detect abnormalities before MRI, which highlights abnormalities according to a combination of the overall effect of biochemical changes on the NMR properties of the water signal, and the sensitivity of the contrast encoding provided by the chosen MRI modality.

High field magnets offer the opportunity to improve the amount, quality, and/or specificity of the information provided by MRS as a direct result of the increased SNR and chemical shift dispersion of the NMR signals. However, the advantages of high field can only be realised if the accompanying disadvantages do not prevail. These include shorter apparent T_2 ($T_2^{\dagger}$) relaxation times [1–3], longer T_1 relaxation times [1], increased main field (B_0) inhomogeneity, increased RF field (B_1) inhomogeneity, greater spatial chemical shift artefacts, and increased eddy current distortions. Nevertheless, it has been demonstrated that, with proper adjustment of all first and second order shims, B_0 inhomogeneity in humans does not prevent improved SNR and spectral resolution for single voxel MRS as field strength is increased up to 7 T [4–6]. The increased B_1 inhomogeneity caused by the field focussing [7] may not pose significant

* Corresponding author. Fax: +44 0 20 7676 2005.
E-mail address: kinchesh@medphys.ucl.ac.uk (P. Kinchesh).

1090-7807/$ - see front matter © 2005 Elsevier Inc. All rights reserved.
doi:10.1016/j.jmr.2005.03.009

problems for single voxel MRS, but ought to be considered for chemical shift imaging (CSI) (MR spectroscopic imaging, MRSI).

MRS voxel localisation is usually achieved by one of three main methods, ISIS (image-selected in vivo spectroscopy [8]), PRESS (point resolved spectroscopy [9,10]), and STEAM (stimulated-echo acquisition mode [11]). For ^{1}H MRS, the biochemical resonances of interest are typically 10^4 times smaller than that of the water signal such that the single shot PRESS or STEAM localisation methods are favoured over ISIS. ISIS requires a combination of eight distinct acquisitions, and relies on cancellation of signals from outside the voxel of interest to achieve the required localisation. As such, ISIS is more sensitive to the effects of physiological motion which, in turn, are more pronounced in the presence of such a relatively large water signal.

For ^{1}H MRS of the human brain, the biochemical metabolite resonances of interest typically exhibit sufficiently long $T_2^\dagger$ relaxation times, on the time scale of short echo-time (TE) single shot sequences, that PRESS is often favoured over STEAM. PRESS is a spin-echo based sequence and, in the absence of relaxation, provides double the signal intensity of the stimulated-echo based STEAM sequence for any given volume. Given that increased SNR is one of the main advantages that high field MRS hopes to exploit, a spin-echo based sequence is arguably the localisation method of choice.

More recently, another single shot spin-echo based sequence, LASER (localisation by adiabatic selective refocusing), has been introduced [12]. LASER uses a non-selective excitation followed by three pairs of adiabatic full-passage (AFP) pulses for signal refocusing and the selection of three orthogonal slices in space, much in the same way as SADLOVE (single shot adiabatic localised volume excitation) [13]. The hyperbolic secant (HS) inversion pulse [14] was the AFP of choice for LASER as the sharp refocusing profiles maximise the signal from the voxel of interest and obviate the need for outer voxel suppression (OVS) which has been considered as a potential source of metabolite signal loss within the voxel of interest via magnetisation transfer [15]. Furthermore, the repetitive application of 180° RF pulses reduces the anti-phase coherence that results from J-coupling, and the effects of diffusion and chemical exchange. As such, the $T_2^\dagger$ increases, just as for a classical Carr–Purcell train. The longer minimum TE of SADLOVE/LASER, in comparison with PRESS, may not, therefore, be a significant disadvantage.

The purpose of this paper is to report the design of a robust SADLOVE/LASER type sequence suitable for clinical spin-echo ^{1}H MRS at high field that uses three pairs of high bandwidth frequency offset corrected inversion (FOCI) pulses for voxel localisation to reduce the chemical shift displacement errors which are magnified at high field. The generation of FOCI pulses is described in a short theory section prior to presenting the sequence and tests of its localisation performance across the spectral range of interest in terms of chemical shift displacement, FOCI pulse efficiency, and outer voxel contamination. Particular attention is also given to the specific choice of excitation pulse.

An important consideration in the practical use of spin-echo MRS is the response from homonuclear J-coupled spins. The anti-phase coherence that is generated by the sequence is therefore compared with that of a conventional PRESS sequence, and the significant improvements that are expected in the case of lactate detection, as a direct result of the reduced chemical shift displacement errors, are described. Another practical consideration is the RF deposition of the sequence and the proposed variants for optimum lactate detection at echo times TE = 144 and 288 ms.

2. Theory

Voxel positioning in localised MRS is normally selected graphically on a set of pilot ^{1}H images. At high field, the greater chemical shift dispersion results in a proportionally greater spatial displacement for the voxel of each metabolite resonance relative to the graphically selected voxel.

For single shot localisation, the fractional displacement ($\Delta x/x$) along each axis, is determined by the bandwidth (BW) of the slice selective RF pulses according to

$$\Delta x/x = \Delta v/\mathrm{BW}, \tag{1}$$

where Δv is the frequency offset of the metabolite resonance and x is the thickness of the slice selected along the axis. In practice, for conventional pulses, the pulse BW is generally limited by the RF power that is available.

Frequency offset corrected inversion (FOCI) pulses [16] are a variant of HS inversion pulses similar in principle to variable-rate selective excitation (VERSE) transformed HS pulses [17]. The VERSE transformation redistributes the RF field (B_1) and RF frequency offset ($\Delta\omega$) of the HS pulse in time by reshaping the temporal B_1 amplitude and $\Delta\omega$ appropriately to reduce the overall specific absorption rate (SAR), which is proportional to B_1^2, whilst maintaining the adiabatic condition. For slice selective inversion, a new (time-varying) slice selection gradient waveform must also be calculated. The variable-rate waveforms are subsequently interpolated to generate uniformly sampled waveforms for prescription. In the case of FOCI pulses, the HS inversion pulse B_1, $\Delta\omega$, and slice selection gradient (G_{HS}) waveforms are simply modulated directly by a suitable function, $A(t)$. The purpose is to increase the BW of the slice selective inversion pulse, whilst maintaining the direction of the effective field such that the pulse remains adiabatic

without having to increase the peak RF power required to fulfil the adiabatic condition. As such, VERSE transformed HS inversion pulses and FOCI pulses can be designed to exhibit very similar properties [18,19]. A consequence of the gradient modulation is that the frequency offset (ω_{offset}) of the base HS pulse must also be suitably modulated. Specifically, for a FOCI pulse of duration t_p centred at $t = 0$:

$$B_1(t) = A(t) \times B_1(0) \times \operatorname{sech}(\beta t), \tag{2}$$

$$\Delta\omega(t) = A(t) \times (-\mu\beta \tanh(\beta t) + \omega_{\text{offset}}), \tag{3}$$

$$G(t) = A(t) \times G_{\text{HS}}, \tag{4}$$

and

$$\text{BW} = f_F \times 2\mu\beta, \tag{5}$$

where β (s^{-1}) and μ are the standard constants of the base HS pulse and define the truncation of the B_1 envelope and squareness of the inversion profile, respectively. f_F is the FOCI factor given by

$$f_F = A(\pm t_p/2). \tag{6}$$

The RF efficiency of FOCI pulses is such that the slice selective inversion bandwidth is generally limited by gradient strength available. "C-shape" FOCI pulses are formulated from a base HS pulse using the chosen f_F according to

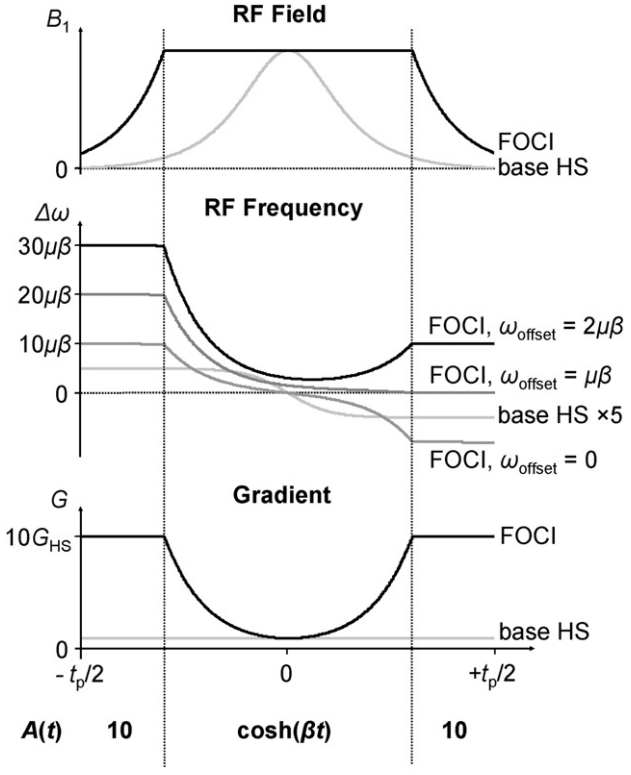

Fig. 1. "C-shape" FOCI pulse waveforms with $f_F = 10$ calculated from a base HS with $\beta = 10/t_p\ s^{-1}$ which gives a B_1 HS cut-off that is 1.35% of the maximum.

$$A(t) = \begin{cases} \cosh(\beta t) & \text{when } \operatorname{sech}(\beta t) > 1/f_F, \\ f_F & \text{otherwise,} \end{cases} \tag{7}$$

and are predicted to generate the sharpest inversion profiles of all the shapes studied [16]. Fig. 1 shows the waveforms generated with $f_F = 10$.

The inversion profiles of FOCI pulses have shown improved slice definition and chemical shift offset behaviour on clinical MR systems [20] but, to our knowledge, have not yet been used to refocus magnetisation in spin-echo generation. A single FOCI pulse is adequate to produce inversion ($-z$ magnetisation) but cannot be used on its own as a refocusing pulse because the phase and echo-time across the selected slice is not uniform. Instead a pair of identical FOCI pulses must be used, the second of which unwinds the phase wrap produced by the first and corrects for the echo-time variation across the selected slice, as for any pair of identical selective adiabatic inversion pulses [21].

3. Sequence design

The L-FOCI (LASER localisation using FOCI pulses) pulse sequence in Fig. 2 was designed for reduced chemical shift displacement errors. A 90° adiabatic half-passage (AHP) is used for excitation and three pairs of FOCI pulses are applied in slice selective gradients (shaded grey in Fig. 2) along three orthogonal axes for voxel selection. Crusher gradient pairs (unshaded in Fig. 2) about each FOCI pulse serve to dephase unwanted signal in each of the slice planes selected by the FOCI pulses, such that only signal generated by the initial excitation pulse and subsequently inverted by each of the FOCI pulses in the RF train is acquired. The crusher gradients ensure that the sequence is a

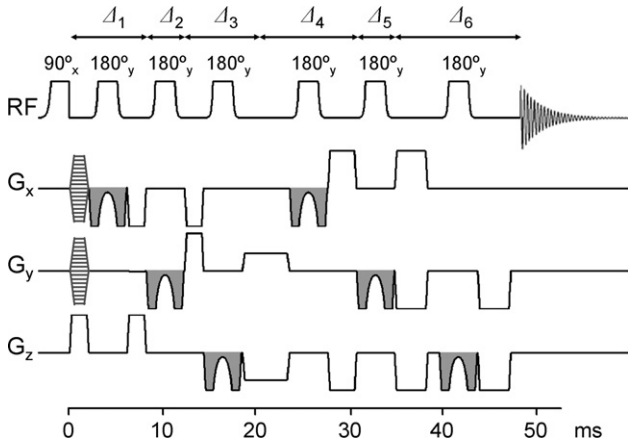

Fig. 2. L-FOCI (LASER localisation using FOCI pulses) pulse sequence using "C-shape" FOCI pulse waveforms with optional phase encoding for 2D chemical shift imaging (CSI). $\Delta_1 = 8$ ms, $\Delta_2 = 4$ ms, $\Delta_3 = 8$ ms, $\Delta_4 = 10.5$ ms, $\Delta_5 = 4$ ms, $\Delta_6 = 13.5$ ms, $\text{TE} = \Delta_1 + \Delta_2 + \Delta_3 + \Delta_4 + \Delta_5 + \Delta_6 = 48$ ms, and $f_F = 10$.

single shot technique, and so phase cycling is not required. In the form presented, the first crusher gradient of each pair is arranged to overlap the second of the preceding pair, to minimise the overall TE, and slice selection is cycled along alternate axes such that the required signal is only ever completely refocused at the onset of acquisition.

All gradient ramps are fixed at 250 μs and the six prescribed pairs of crusher gradient strengths are ±34.2 mT/m along each axis, with plateau durations of 1.5, 1.5, 1.5, 2.5, 2.5, and 3 ms, respectively. The overlap of crusher gradients necessitates that the longest crusher gradient duration takes precedence, and the overlapping crusher is balanced accordingly, except for between the 3rd and 4th inversion pulses where both crushers are balanced to fill the time available. Provided no signal is observed if any one of the RF pulses is turned off, the only possible source of signal contamination is from stimulated echoes that are generated by the initial excitation pulse and subsequently perturbed by all of the following pulses. Although the variation in interpulse delays has the potential to generate stimulated echoes with first order phase anomalies, their contribution is considered to be negligible due to a combination of the efficiency of adiabatic inversion and improper gradient refocusing for stimulated-echo formation. The minimum TE was determined by careful experimentation to ensure adequate crusher gradient strengths and durations are used in vivo. It is perhaps surprising that this is not achieved when all of the interpulse delays are equal. We can only imagine that this is because the phase is not uniform across the slice selected by the first pulse of any AFP pair, and so not so much crushing is required to destroy the unwanted coherences.

Phase can be encoded into the signal at the same time as the first crusher gradient in two mutually orthogonal directions for 2D CSI without any penalty in overall TE (in vivo CSI is often performed on a PRESS selected volume). An imaging option (not shown), with echo formation in the centre of the acquisition window and in the presence of a "read-out" gradient along either G_x, G_y or G_z, was also incorporated in the sequence. TE can be increased either by extending any of the components or by inserting additional pairs of non-selective inversion pulses immediately after the initial excitation pulse to maximise $T_2^{\dagger}$, as with CP-LASER [3]. If TE is increased by significantly extending any of the interpulse durations then the corresponding crusher gradients should not overlap but rather flank their respective FOCI pulses to minimise diffusion encoding. Optional incremental delays either side of the final 180° pulse enable a 2D *J*-resolved spectrum to be acquired from the localised volume, in the same way as for PRESS [22].

The sequence was implemented and tested on an imaging spectrometer supplied by *Philips Medical Systems* and based on a MR5000 design by *SMIS Ltd, UK*. The spectrometer was equipped with a 4.7 T, 90 cm bore magnet (*Magnex Scientific Ltd, UK*), a 38 cm bore shielded head gradient coil giving gradients up to 36 mT/m with a maximum slew rate of 195 mT/m/ms (*Magnex Scientific Ltd, UK*), a transmit/receive four-port drive birdcage RF coil with internal diameter 28 cm [23], and 4 kW RF amplifier (*Communication Power Corporation, NY*).

4. Localisation performance

The localisation performance of L-FOCI was tested in terms of chemical shift displacement errors by comparison with a conventional PRESS sequence. Since each FOCI pulse frequency waveform can only be prescribed precisely for a single spectral offset the localisation performance was also tested across the ^{1}H spectral range of interest in terms of FOCI pulse efficiency and outer voxel contamination. A hard 90° excitation pulse of duration 250 μs was used in the performance tests as the excitation produced by this pulse is essentially uniform and in-phase across the spectral range of interest (following a small first order phase correction that can be eliminated by judicious choice of experimental timing). The performance and merits of various adiabatic excitation schemes will be considered in the next section. Normally, only the ^{1}H brain metabolite resonances up field of the water signal (from 1.25 to 4.25 ppm [24]) are analysed [25,26], corresponding to a 600 Hz range at 4.7 T.

The shortest 5 lobe sinc pulses that could possibly be used for the 90° and 180° localisation pulses of PRESS were determined to be 0.669 ms (BW = 9 kHz) and 1.2 ms (BW = 4 kHz), respectively, as limited by RF power. This could only be achieved for a favourably positioned voxel by overdriving the 4 kW RF amplifier and prescribing reduced flip angles. If the RF power is strictly limited to 4 kW and 90° and 180° localisation pulses are used, the shortest 5 lobe sinc pulses that could be used in vivo under favourable conditions would be 1 ms (BW = 6 kHz) and 2 ms (BW = 2.2 kHz), respectively. The 1.2 ms (BW = 4 kHz) sinc pulse that can only be prescribed properly with considerably increased RF power is used to demonstrate just how effective L-FOCI is at reducing chemical shift displacement errors with respect to PRESS.

Fig. 3 illustrates the effect of a 600 Hz resonance offset on the volume selected by PRESS and L-FOCI refocusing schemes using a 1.2 ms sinc pulse and a pair of 2.5 ms "C-shape" FOCI pulses (BW = 20 kHz, $f_F = 10$, base HS: $\mu = 1.67$, $\beta = 4000\ s^{-1}$), respectively. OVS was used to suppress the side lobes generated by the 1.2 ms sinc pulse. The chequered pattern in the images of the voxels selected by FOCI pulses in Fig. 3B is caused by an RF amplitude cut-off level that is

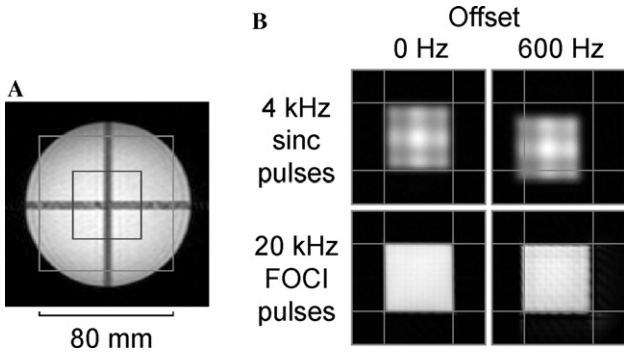

Fig. 3. (A) 120 mm × 120 mm pilot image of a spherical phantom showing 80 mm × 80 mm image field of view (FOV) for the images in B, and graphical location of 40 mm × 40 mm in-plane PRESS and L-FOCI (LASER localisation using FOCI pulses) selected voxels. The dark vertical and horizontal bands in the image are saturation bands from two orthogonal slices that were also acquired in the pilot scan. (B) Comparison of 80 mm × 80 mm images showing 40 mm × 40 mm in-plane voxel selection using sinc and FOCI refocusing schemes with signals on-resonance and offset by 600 Hz. Slice thickness = 10 mm. The guide-lines illustrate the position of the graphically selected voxel.

13.5% of the maximum value for the FOCI pulses (Fig. 1). This can be largely eliminated with negligible loss in performance by recasting Eq. (2) according to

$$B_1(t) = A(t) \times B_1(0) \times \{\mathrm{sech}(\beta t) - \mathrm{sech}(\beta t_p/2)\} \qquad (8)$$

such that the cut-off is removed, as reported for other pulse shapes [27].

For lactate, the CH ($\delta = 4.1$ ppm) and CH_3 ($\delta = 1.3$ ppm) [24] PRESS selected voxels using the highest BW sinc pulses possible have a common volume that is only 69% of the voxel size selected. For properly calibrated 90° and 180° localisation pulses and prescription within the 4 kW limit, the common volume would be reduced to 50%. This has important implications regarding the amount of signal that is observed for the *J*-coupled spins [28–34], as will be discussed in more detail. For L-FOCI, the common volume is increased to 92% by using three pairs of 20 kHz FOCI pulses for voxel localisation.

Having demonstrated the significant reduction in chemical shift displacement errors that are possible with L-FOCI preliminary in vivo testing was performed with the RF amplifier strictly limited to 4 kW. FOCI pulse durations were subsequently increased to 3.5 ms (BW = 20 kHz, $f_F = 10$, base HS: $\mu = 2.33$, $\beta = 2857.1\ s^{-1}$) to ensure the adiabatic condition is routinely met in vivo. The efficiency of L-FOCI was then tested across the ^1H spectral range of interest at 4.7 T.

Fig. 4 shows the L-FOCI profiles generated from a signal at specific spectral offsets from an on-resonance water signal across the spectral range of interest. FOCI pulses were prescribed correctly for a signal at 2.75 ppm, corresponding to the centre of the spectral range of interest, and the 250 μs hard pulse was applied on-resonance. The total intensity and outer voxel contamination (OVC) at each offset were measured from the magnitude data after subtracting the mean noise level calculated from the first and last 25 points of all the profiles, and thresholding to leave only a single 'island' of data. Data inside and outside the 'island' for each profile were subsequently summed and combined to give the total intensity which was then normalised according to the profile with maximum intensity. The slight loss in signal intensity about the centre of the spectral range of interest is in good agreement with experimental FOCI pulse data at an offset of 250 Hz [20] and simulated FOCI pulse data at an offset of 500 Hz [16]. These losses will be largely compensated for by the use of spectral analysis routines such as LCModel [25,26] which require a basis set of metabolite spectra recorded under identical conditions to model in vivo data. The basis set of in vitro metabolite spectra is scaled consistently with each other using a common marker and will, therefore, likewise reflect the L-FOCI intensity distribution across the spectral range.

The level of total OVC corresponds to the one dimension of each profile. For three dimensional localisation, it is anticipated that the total outer volume contamination will be approximately three times greater, i.e.,

Offset /Hz	-800	-700	-600	-500	-400	-300	-200	-100	0
Total Intensity /%	98.4	99.0	99.8	100.0	100.0	99.6	98.8	97.9	96.1
Total *OVC* /%	0.10	0.11	0.15	0.15	0.13	0.13	0.09	0.14	0.12
$OVC(0 \rightarrow 0.1x)$ /%	0.07	0.06	0.08	0.08	0.07	0.08	0.06	0.08	0.09
$OVC(0.1x \rightarrow 0.2x)$ /%	0.02	0.04	0.05	0.03	0.02	0.02	0.03	0.02	0.01

Fig. 4. L-FOCI (LASER localisation using FOCI pulses) profiles generated from a signal at the specified spectral offset. Cut-off removed FOCI pulses were prescribed correctly for a signal with a spectral offset of −390 Hz (corresponding to 2.75 ppm at 4.7 T for an on-resonance water signal). A 250 μs on-resonance hard pulse was used for excitation and a pair of 3.5 ms "C-shape" FOCI pulses (BW = 20 kHz, $f_F = 10$, base HS: $\mu = 2.33$, $\beta = 2857.1\ s^{-1}$) for refocusing. Slice thickness (x) = 15 mm. Number of data points per profile = 1024. The total intensity and total outer voxel contamination (OVC) at each offset are given. $OVC(0 \rightarrow 0.1x)$ corresponds to the level of OVC that lies in the regions immediately outside of each slice and up to a distance equal to $0.1x$ whilst $OVC(0.1x \rightarrow 0.2x)$ corresponds to the level of OVC that lies in the regions between distances of $0.1x$ and $0.2x$ from the edges of each slice.

within 0.5% across the spectral range of interest at 4.7 T. OVC$(0 \rightarrow 0.1x)$ corresponds to the level of OVC that lies in the regions immediately outside of each 'island' and up to a distance equal to $0.1x$ whilst OVC$(0.1x \rightarrow 0.2x)$ corresponds to the level of OVC that lies in the regions between distances of $0.1x$ and $0.2x$ from the edges of each 'island.' The data demonstrate that OVC is concentrated in regions close to the prescribed voxel in agreement with theoretical calculations. As such, the in vivo OVC is expected to be of a similar magnitude despite the four- to fivefold increase in subject-to-voxel active volume ratio inherent to studies of the adult human brain.

5. Excitation pulse

The initial tests of L-FOCI were performed using a 250 μs hard pulse for excitation because of the uniformity of the excitation envelope across the spectral range. However, just as with both SADLOVE and LASER sequences, an adiabatic excitation pulse that eliminates signal loss resulting from any intra-voxel B_1 inhomogeneity is preferable, particularly as calibration is not required. The excitation envelopes produced by HS, 'FOCI,' and tanh/tan [35] AHPs, and subsequently BIR-4 [35] 90° pulses (HS, 'FOCI,' and tanh/tan variants) were calculated by the progressive step-wise rotation of initial equilibrium magnetisation about the effective field (B_{eff}) generated by the RF waveforms as a function of spectral offset. B_1 values up to 1414 Hz were considered appropriate for the 4 kW RF amplifier following accurate calibration of the 90° 250 μs hard pulse ($B_1 = 1000$ Hz) which was measured to correspond to 2.0 kW of output power. BIR-4 90° pulses were considered to be of particular interest because of the wide excitation BW that they are reported to exhibit [35].

Fig. 5 compares the calculated excitation envelopes of some HS AHPs with maximum B_1 values of 1000 Hz (=2 kW), 1225 Hz (=3 kW), and 1414 Hz (=4 kW). The pulse duration was fixed to 3.2 ms and cut-offs were removed in the same manner as described previously. Doubling the pulse duration to 6.4 ms did not significantly modify the calculated performance of the AHPs. The calculated excitation envelope for the HS AHP of Fig. 5A ($\mu = 2.13$, $\beta = 1472.6\ \text{s}^{-1}$) shows that the BW of this AHP is not wide enough to cover the spectral range of interest, with gross variation in both magnitude and phase at offsets below −100 Hz. Increasing the value of μ (and therefore the BW) by a factor of 5 to give the HS AHP of Fig. 5B ($\mu = 10.67$, $\beta = 1472.6\ \text{s}^{-1}$) reduces the variation but the maximum of the excitation envelope's magnitude drifts increasingly off-resonance and an increasing amount of first order phase correction is required for the lower values of B_1. Reducing β by a factor of 5 and increasing μ accordingly increases the average B_1 and gives the HS AHP of Fig. 5C ($\mu = 53.33$, $\beta = 294.5\ \text{s}^{-1}$). Whilst the calculated performance of this pulse is arguably better than that of the pulse in Fig. 5B, the HS8 [36] AHP in Fig. 5D ($\mu = 10.67$, $\beta = 1472.6\ \text{s}^{-1}$) is calculated to result in smaller variations in magnitude and phase across the spectral range of interest.

Fig. 6 shows the calculated excitation envelopes of a cut-off removed 'FOCI' AHP ($f_F = 10$, base HS: $\mu = 10.67$, $\beta = 1472.6\ \text{s}^{-1}$) generated from the base HS AHP of Fig. 5A and a tanh/tan AHP ($\Delta\omega_{\max} = 15$ kHz, $\zeta = 10$, and $\tan[\kappa] = 20$ for the modulation functions defined in [35]) that is considered to be close to optimal for non-selective excitation. The calculated performance of the 'FOCI' AHP in Fig. 6A is considered to be marginally better than that of the HS8 AHP in Fig. 5D, in terms of both magnitude and phase, and marginally worse, only in terms of phase, than the close to optimal tanh/tan AHP in Fig. 6B. The calculated performance of

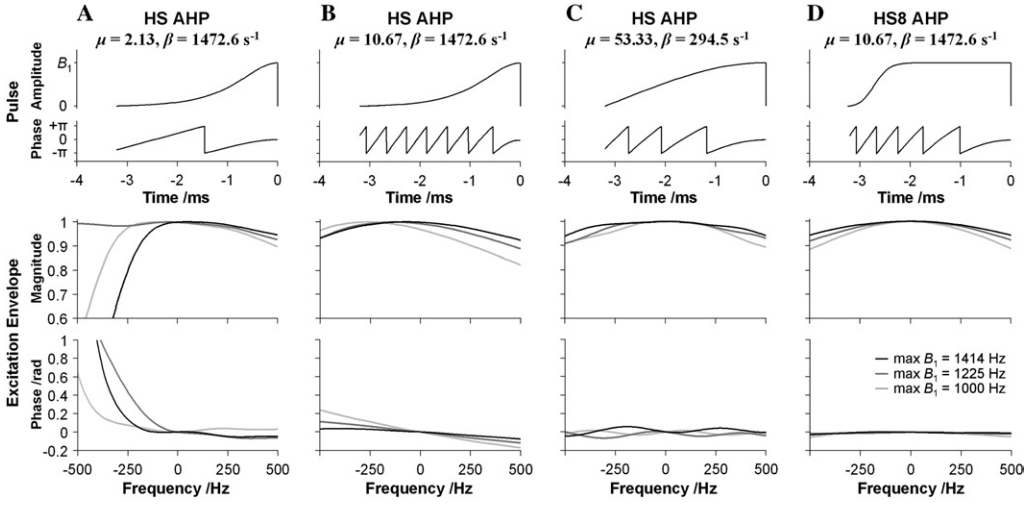

Fig. 5. Calculated excitation envelopes for some 3.2 ms HS AHPs that were generated from the given parameters.

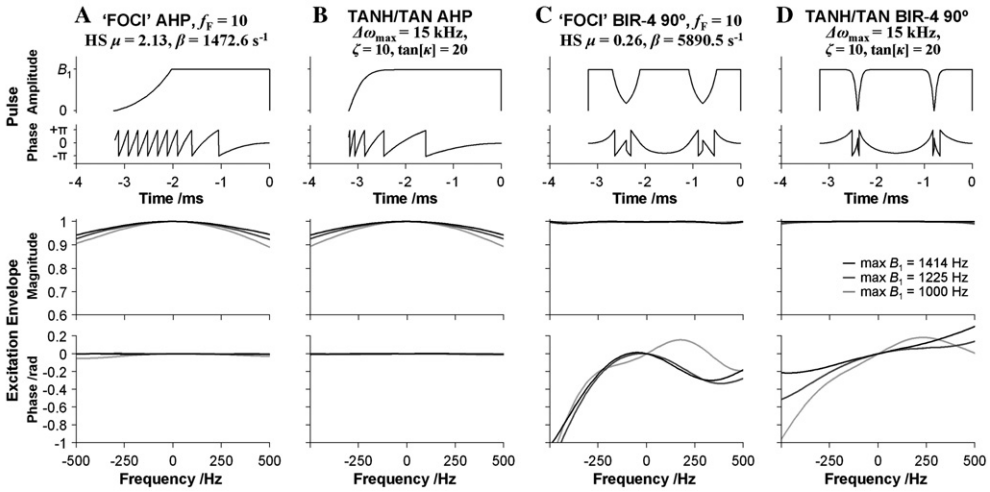

Fig. 6. Calculated excitation envelopes for some 3.2 ms 'FOCI' and tanh/tan excitation pulses that were generated from the given parameters. The tanh/tan modulation functions that use the parameters $\Delta\omega_{max}$, ζ, and tan[κ] are defined in [35].

the 'FOCI' BIR-4 90° pulse ($f_F = 10$, base HS: $\mu = 0.26$, $\beta = 5890.5\ s^{-1}$) and tanh/tan BIR-4 90° pulse ($\Delta\omega_{max} = 15$ kHz, $\zeta = 10$, and tan[κ] = 20) in Figs. 6C and D, respectively, confirm that, for the B_1 values of interest, BIR-4 90° excitations are typically uniform over a significantly wider BW than AHPs. However, the calculated phase performance, which was subsequently verified experimentally for the 'FOCI' BIR-4 90° pulse, is not so good, even after optimum first order phase correction.

The excitation pulse currently deployed is the 'FOCI' AHP in Fig. 6A. The calculated magnitude of the excitation envelope between frequencies ±300 Hz off-resonance that can cover the 600 Hz spectral range of interest at 4.7 T is symmetric about the transmitter offset, decreasing with increasing offset to 95.6% for maximum $B_1 =$ 1000 Hz, to 97.0% for maximum $B_1 = 1225$ Hz, and to 97.7% for maximum $B_1 = 1414$ Hz. The phase across the same range is calculated to be uniform to within 1.75° for $B_1 = 1000$ Hz, to within 0.62° for $B_1 =$ 1225 Hz, and to within 0.39° for $B_1 = 1414$ Hz.

The experimental performance of the 'FOCI' AHP in Fig. 6A was tested with transmitter offset set to −390 Hz with respect to an on-resonance water signal. At 4.7 T, this corresponds to the centre of the spectral range of interest at 2.75 ppm. The experimental performance is compared with that of an accurately calibrated on-resonance 250 μs hard pulse in Fig. 7. Cut-off removed FOCI AFPs were prescribed correctly for localisation of a signal at the centre of the spectral range of interest for both excitation schemes. The experimental data for the 'FOCI' AHP are in good agreement with the calculated excitation envelope after allowing for the FOCI AFP losses across the spectral range that are reflected in the experimental data of the hard pulse. The 'FOCI' AHP produces more signal than the accurately calibrated hard pulse, presumably due to intra-voxel B_1 inhomogeneity. The relative performance of the 'FOCI' AHP is expected to be even better in vivo due to both increased intra-voxel B_1 inhomogeneity and reduced precision of hard pulse calibration. With 'FOCI' AHP prescription in the 2–4 kW range, the magnitude of the excitation envelope is calculated to differ by less than 2.1% at the edge of the spectral range and spectral fitting of in vitro spectra using LCModel is not, therefore, expected to be overly compromised by the in vivo field focusing.

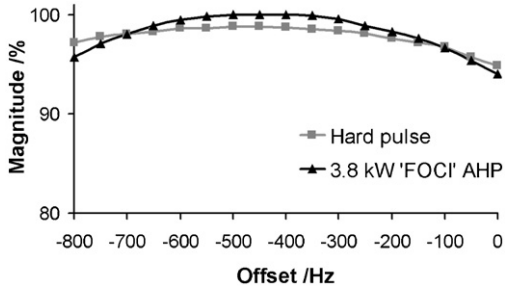

Fig. 7. L-FOCI (LASER localisation using FOCI pulses) magnitude data generated from a signal as a function of spectral offset for excitation with an on-resonance 250 μs hard pulse (grey), and a cut-off removed 3.2 ms 'C-shape FOCI' AHP ($f_F = 10$, base HS: $\mu = 2.133$, $\beta = 1472.6\ s^{-1}$) with transmitter offset = −390 Hz (black). A 15 mm × 15 mm × 15 mm voxel was localised at the centre of a spherical phantom with cut-off removed FOCI pulses prescribed correctly for a signal with a spectral offset of −390 Hz.

6. Homonuclear *J*-coupled spins

The TE of 48 ms, with the timing as given in the pulse sequence diagram of Fig. 2, was determined to be the minimum TE that could be used in vivo whilst ensuring true single shot performance. Lower TE could only be achieved with a suitable phase cycling scheme to cancel

unwanted coherences, but is not so suitable for in vivo applications. This is in good agreement with a quantitative short echo-time study using LASER, TE = 46 ms, and a quadrature birdcage coil at 4 T [15]. It was not possible to obtain single shot performance with TE = 36 ms and replication of the timing scheme and crusher gradient values used in a surface coil study at 4 T [12]. Presumably, the range of the surface coil results in a significant reduction in unwanted coherences that can be detected.

Having demonstrated the reduced chemical shift displacement errors of L-FOCI and good performance across the spectral range of interest, we now consider the effects of homonuclear *J*-coupling. There should be no problem in detecting metabolites that exhibit characteristic singlets as they will remain in-phase irrespective of the timing scheme. It is, however, important to consider the response from key metabolites that are characterised purely by homonuclear *J*-coupled spins, such as the excitatory and inhibitory neurotransmitters, glutamate (Glu) and γ-aminobutyric acid (GABA). The coupling pattern of glutamate was calculated at 4.7 T for L-FOCI with TE = 48 ms using the GAMMA magnetic resonance simulation platform [37] and published chemical shifts and coupling constants [24]. Data were calculated with Lorentzian lineshapes and linewidths up to those typically encountered in vivo assuming ideal 'delta function' pulses and neglecting relaxation. The signals from outside of the volume that is common to all spins were ignored for two reasons. First, they exhibit less phase modulation than the signal from the common volume and, second, localisation pulses with a BW of 20 kHz ensure that the fractional displacement of voxels is very small. The results are compared with those for a simple pulse and acquire sequence and a symmetric PRESS sequence ($TE = \Delta_1 + \Delta_2$, $\Delta_1 = \Delta_2$) with TE = 32 and 48 ms in Fig. 8.

The calculations clearly demonstrate that the glutamate spectrum contains signals that remain strongly coupled at 4.7 T, and that L-FOCI with TE = 48 ms results in a significant reduction in the anti-phase coherence from *J*-coupling when compared to PRESS with TE = 48 ms. Indeed, for many metabolites, data for L-FOCI with TE = 48 ms can perhaps be more reasonably compared to those of a symmetric PRESS sequence with TE = 32 ms (data for a comprehensive range of metabolites are published at http://www.medphys.ucl.ac.uk/~kinchesh/l-foci). One notable exception is lactate (Lac), for which the L-FOCI with TE = 48 ms response is essentially the same as for a symmetric PRESS sequence with TE = 48 ms, as shown in Fig. 9.

Lactate detection is usually performed using the doublet of the CH_3 group at 1.3 ppm. At short TE, this region of the spectrum is complicated by macromolecular resonances such that observation is often performed at longer TE. A number of timing schemes have been proposed to optimise detection for the PRESS sequence [28–34]. A density matrix treatment based on first principles [38] using ideal 'delta-function' pulses and a weakly coupled two spin system in the absence of relaxation confirms the analysis that has been presented for each of the distinct regions as defined by perfectly

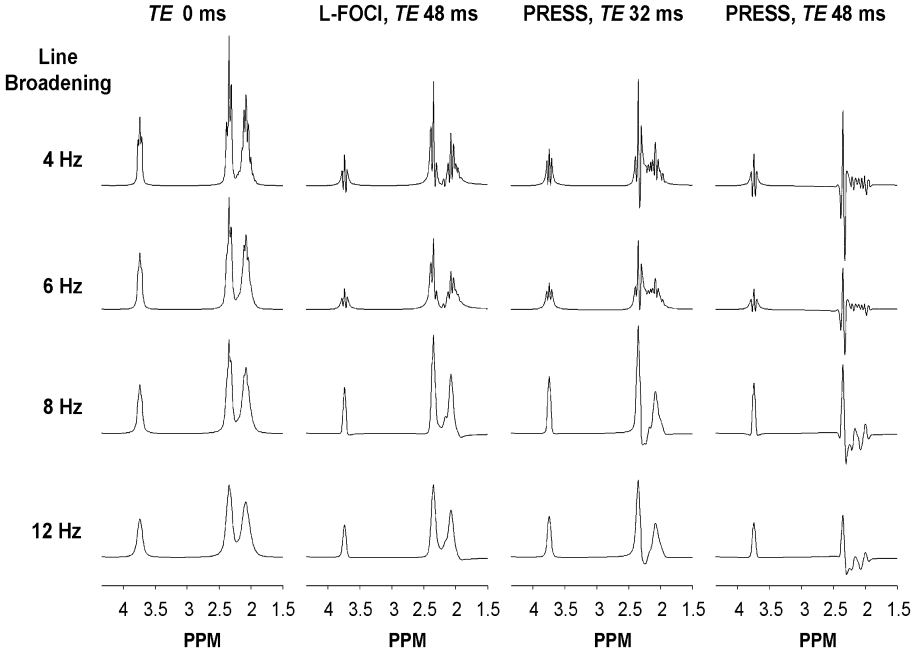

Fig. 8. Calculated coupling patterns of glutamate (Glu) at 4.7 T for the following sequences: pulse and acquire (TE = 0 ms), L-FOCI (LASER localisation using FOCI pulses, TE = 48 ms, timing scheme as in Fig. 2), and symmetric PRESS (TE = 32 and 48 ms). Data are presented on the same vertical scale with Lorentzian lineshapes and linewidths as indicated. Ideal pulses were assumed and relaxation was neglected.

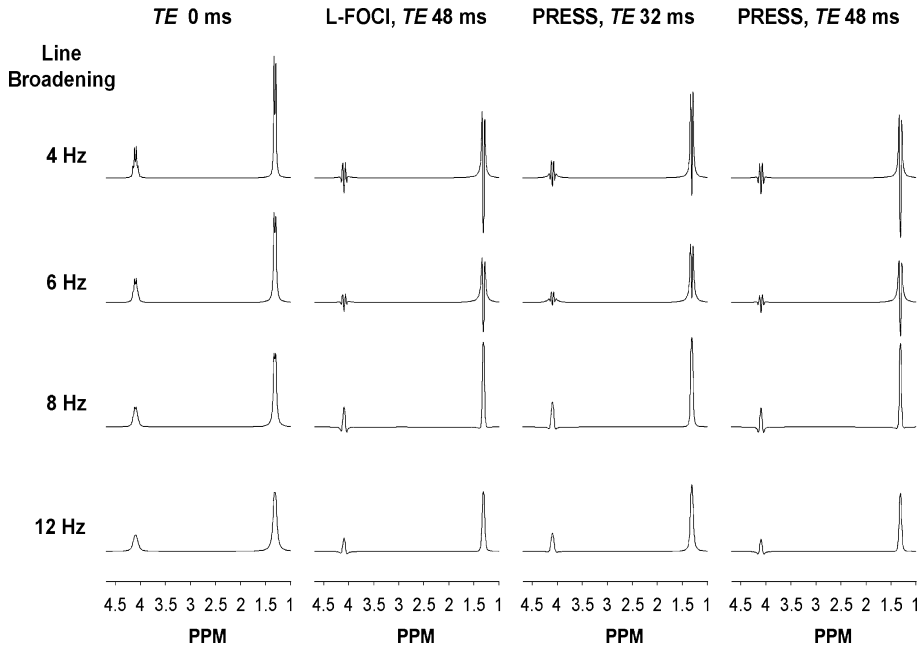

Fig. 9. Calculated coupling patterns of lactate (Lac) at 4.7 T for the following sequences: pulse and acquire (TE = 0 ms), L-FOCI (LASER localisation using FOCI pulses, TE = 48 ms, timing scheme as in Fig. 2), and symmetric PRESS (TE = 32 and 48 ms). Data are presented on the same vertical scale with Lorentzian lineshapes and linewidths as indicated. Ideal pulses were assumed and relaxation was neglected.

rectangular slice selection in an 'ideal' PRESS experiment [31].

At TE = 144 ms ($1/J$), symmetric ($\Delta_1 = \Delta_2$) and asymmetric ($\Delta_1 \neq \Delta_2$) sequences perform equally well but the inverted doublet suffers signal loss, the magnitude of which depends entirely on the fractional displacement in two dimensions resulting from the BW of the 180° pulses. Contributions to the spectrum from outside of the common volume selected by the two 180° pulses either cancel completely or, for the small volume in which only the CH_3 group is localised by the 180° pulses, result in an upright doublet that subtracts from the inverted doublet. For a PRESS sequence with 4 kHz BW 180° pulses, it is therefore predicted that approximately 72% of the desired signal is actually detected to be inverted at 4.7 T. For 2.2 kHz BW 180° pulses, the corresponding value is only 49%. For L-FOCI, the density matrix treatment can readily be extended by inspection, and it is not difficult (albeit rather tedious) to demonstrate the somewhat intuitive result that, for L-FOCI, the size of the inverted signal is approximately equal to the common volume, which corresponds to 92% for 20 kHz BW FOCI pulses at 4.7 T. Additional losses that result from the 'non-ideal' experimental slice profiles are likely to be greater for PRESS.

At TE = 288 ms ($2/J$), asymmetric PRESS with $\Delta_1 \to 0$ (or $\Delta_2 \to 0$) performs significantly better than symmetric PRESS with all contributions from outside of the common volume adding to the upright doublet. However, these contributions are not completely in-phase because it is not possible to set Δ_1 or Δ_2 exactly to zero in a conventional PRESS sequence. At TE = 576 ms ($4/J$), all contributions within and outside of the common volume result in an upright doublet with symmetric PRESS, and there is no signal loss arising from chemical shift displacement errors.

The inherent signal loss at TE = $1/J$ has resulted in the use of TE = $2/J$ and $4/J$ spectra for lactate quantitation at 2.4 T [39]. At 4.7 T, however, significant $T_2^{\dagger}$ losses occur with TE = $4/J$ such that use of data at TE = $1/J$ becomes much more favourable. The $T_2^{\dagger}$ losses can be further minimised by the use of CP-LASER type sequences. Indeed, it has been demonstrated that, for the non-exchanging methyl protons in NAA and Cr, the use of CP-LASER as opposed to PRESS increases $T_2^{\dagger}$ by factors of 1.7 and 1.8, respectively, at 4 T, and by factors of 2.2 and 2.0, respectively, at 7 T [3]. Whilst the benefits of CP-LASER type sequences over LASER type sequences may not be so pronounced, they are still expected to significantly enhance the observed signal, particularly for TE = $2/J$.

For optimal lactate detection with L-FOCI at longer TE, we therefore propose the following schemes at 4.7 T. At TE = 144 ms, three blocks of inversion pulses, each with TE = 48 ms and six inversion pulses timed as in Fig. 2, and voxel selection performed exclusively in the last block. The non-selective inversion pulses in the first two blocks only require a BW suitable to cover the spectral range of interest so that the SAR can be minimised. A suitable pulse would be a 3.5 ms HS pulse with BW = 2 kHz, $\mu = 2.33$, and $\beta = 2692.8\ s^{-1}$. This pulse is calculated to give better than 99% inversion

across the spectral range of interest when prescribed with maximum $B_1 \geqslant 1110$ Hz. The small signal contributions from outside of the common volume will all modulate to produce observable magnetisation at $\omega \pm 1/2J = \exp(\pm i\varphi)$ with $2\pi/3 = \varphi < \pi$ so that they tend to contribute to, rather than cancel from, the inverted doublet of the common volume. The non-selective inversion pulses in the first two blocks should also increase $T_2^{\dagger}$ and, therefore, the size of the observed signal. A GAMMA calculation of the lactate coupling pattern at 4.7 T using published chemical shifts and $J = 6.993$ Hz [24] confirmed that, for L-FOCI with TE = 144 ms and the proposed timing scheme comprising three blocks of six inversion pulses as described, the doublet is properly inverted.

At TE = 288 ms, we suggest the same strategy but with six blocks of inversion pulses to give magnetisation at $\omega \pm 1/2J = \exp(\pm i\varphi)$ with $5\pi/3 \geqslant \varphi \geqslant 2\pi$. For quantitation purposes, it should be possible to extrapolate back to TE = 0 assuming that $T_2^{\dagger}$ decays mono-exponentially with each block of inversion pulses. Only a small correction factor would be required to correct for the slight anti-phase coherence that is common to the signals in both measurements. Although there are obvious reservations in using dual-echo data in this manner, particularly in vivo [40], it is encouraging to note that ^{1}H metabolite T_2 relaxation at 3 T within a TE range of 50–450 ms was observed to be purely mono-exponential for all the investigated singlets [41]. Clearly, data at additional TE would be preferable should clinical examination times permit.

For lactate detection at longer TE with LASER/CP-LASER type sequences, GAMMA calculations show that some degree of consideration should be given to the exact TE at which the doublet is properly inverted (or properly upright). Fig. 10 shows the calculated TE at which the lactate doublet at 1.3 ppm is properly inverted as a function of the number of equally spaced ideal refocusing pulses at 1.5, 3, and 4.7 T. It should, however, be noted that the use of real refocusing pulses could result in deviation from the predicted behaviour presented.

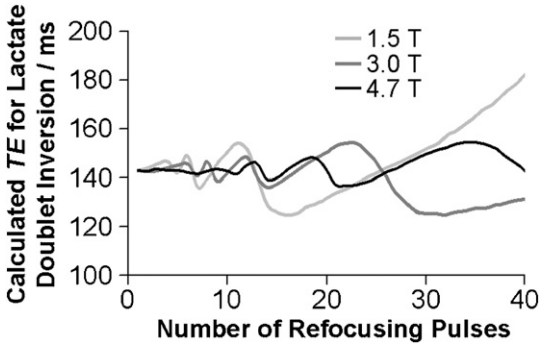

Fig. 10. Calculated TE at which the lactate doublet at 1.3 ppm is properly inverted as a function of the number of equally spaced ideal refocusing pulses at 1.5, 3, and 4.7 T.

7. RF deposition

A consequence of using a pair of adiabatic pulses for slice selective refocusing as opposed to more conventional RF pulses is the increased RF power requirement. The relative RF pulse power of various adiabatic and conventional pulses is calculated to compare the RF deposition of spin-echo MRS sequences and assess the impact of working within the Medical Devices Agency (MDA) safety guideline of 4 W/kg as the maximum acceptable SAR over the whole human head [42]. Simulations have shown that if this guideline is adhered to the guideline of 10 W/kg for any 100 g of tissue is unlikely to be exceeded with a four-port drive birdcage RF coil [43].

Table 1 compares the RF pulse power of some adiabatic and conventional pulses relative to a 250 μs hard 90° pulse for which $B_1 = 1000$ Hz (pulse A). With a given upper limit of $B_1 = 1414$ Hz a 1 ms of 5 lobe sinc 90° pulse, for which the maximum prescribed $B_1 = 1407$ Hz (pulse B), corresponds to the shortest 5 lobe sinc 90° pulse that can be used in vivo under favourable conditions in a PRESS sequence. The corresponding 180° pulse is 2 ms with BW = 2.2 kHz (pulse C). The HS AFP with approximately the same BW (pulse D) is calculated to produce greater than 99% inversion with a maximum prescribed $B_1 = 1110$ Hz. Application of the pulse with a suitably higher B_1 makes it immune to field focussing effects and obviates the need for pulse calibration. The tabulated relative power is therefore calculated for prescription with a maximum B_1 at the upper limit of 1414 Hz. Although these sinc and HS 180° pulses both produce inversion across a similar BW, the AFP requires over twice as much power. The slice selective FOCI pulse with BW = 20 kHz (pulse E) that is generated with $f_F = 10$ from this base HS AFP produces greater than 99% inversion at the same maximum prescribed $B_1 = 1110$ Hz, but the 10-fold increase in BW only requires about 3.5 times as much power. This is in contrast to the HS AFP with BW = 20 kHz and the same pulse duration (pulse F) which is calculated to produce greater than 99% inversion with a maximum prescribed $B_1 = 3750$ Hz and requires about 10 times as much power. Although the 3.5 ms HS8 AFP with BW = 20 kHz (pulse G) is calculated to produce greater than 99% inversion with a maximum prescribed $B_1 = 1960$ Hz, the relative power of this pulse is slightly greater than that of the HS AFP with BW = 20 kHz. Reducing the BW of the slice selective FOCI pulse from 20 to 10 kHz (pulse H) reduces the FOCI pulse power by a factor of 2.5. The HS8, 'FOCI,' and tanh/tan AHPs described previously as suitable excitation schemes are

Table 1
Relative power requirements of adiabatic[a] and conventional pulses

	RF pulse	Flip (rad)	Pulse duration (ms)	BW[b] (kHz)	f_F	μ_{HS}[c]	β_{HS}[c] (s^{-1})	Maximum applied B_1[d] (Hz)	Relative RF power
A	Hard pulse	π/2	0.25	—	—	—	—	1000	1.00
B	5 lobe sinc	π/2	1.0	6.0	—	—	—	1407	1.27
C	5 lobe sinc	π	2.0	2.2	—	—	—	1407	2.53
D	HS AFP	π	3.5	2.0	—	2.33	2692.8	1414 (1110)	5.79
E	FOCI AFP	π	3.5	20.0	10	2.33	2692.8	1414 (1110)	19.82
F	HS AFP	π	3.5	20.0	—	23.33	2692.8	4777 (3750)	66.04
G	HS8 AFP	π	3.5	20.0	—	46.67	1346.4	2496 (1960)	68.78
H	FOCI AFP	π	3.5	10.0	10	1.17	2692.8	943 (740)	8.81
I	HS8 AHP	π/2	3.2	—	—	10.67	1472.6	1414	19.96
J	'FOCI' AHP	π/2	3.2	—	10	2.13	1472.6	1414	18.11
K	tanh/tan AHP[e]	π/2	3.2	—	—	—	—	1414	22.88
L	Gaussian	π/2	32.0	—	—	—	—	<20	<0.02

[a] The values presented correspond to cut-off removed adiabatic pulses.
[b] The BW given for suitable slice selective pulses corresponds to the full width at half maximum.
[c] μ_{HS} and β_{HS} correspond to μ and β of the base HS pulse used to generate the pulses.
[d] The B_1 values in parentheses correspond to the B_1 required for AFPs to achieve >99% inversion.
[e] The tanh/tan AHP was generated with $\Delta\omega_{max} = 15$ kHz, $\zeta = 10$, and $\tan[\kappa] = 20$ using the modulation functions defined in [35].

Table 2
Relative power requirements of some spin-echo MRS sequences

RF pulse sequence[a]	BW[b] (kHz)	RF pulses	Relative RF power	Minimum TR[c] (s)
PRESS[d]	2.2	$7\times B + 2\times C$	13.9	0.3
L-HS	2.0	$J + 6\times D$	52.8	1.0
L-HS	20.0	$J + 6\times F$	414.4	7.6
L-HS8	20.0	$J + 6\times G$	430.8	7.9
L-FOCI	20.0	$J + 6\times E$	137.0	2.5
L-FOCI	10.0	$J + 6\times H$	71.0	1.3
L-FOCI, TE = 144 ms	20.0	$J + 12\times D + 6\times E$	206.4	3.8
L-FOCI, TE = 288 ms	20.0	$J + 30\times D + 6\times E$	310.6	5.7
L-FOCI, TE = 144 ms	10.0	$J + 12\times D + 6\times E$	140.4	2.6
L-FOCI, TE = 288 ms	10.0	$J + 30\times D + 6\times E$	244.6	4.5

[a] L-HS, L-HS8, and L-FOCI represent LASER localisation using HS, HS8, and FOCI pulses.
[b] The BW is given for slice selective π pulses.
[c] The minimum TR is for studies of the typical adult human brain.
[d] Calculation for the PRESS sequence includes six OVS π/2 sinc pulses.

included for comparison (pulses I, J, and K) whilst the 32 ms Gaussian 90° pulse (pulse L) demonstrates that any water suppression scheme using a train of relatively long pulses will contribute negligibly to the overall RF deposition of any MRS sequence.

The building blocks are now in place for a comparison of the overall RF deposition of spin-echo MRS sequences. Table 2 summarises the calculations for various sequences using the pulses in Table 1 and includes the minimum repetition time (TR) that can be used in studies of the adult human brain whilst maintaining the SAR of each sequence within MDA guidelines. For quantitation purposes, it is preferable to scan with a TR that permits nearly full T_1 relaxation. The T_1 relaxation times of major brain metabolites are reported to be in the 0.9–1.6 s range in the brain regions studied at 3 T [44]. All of the proposed L-FOCI sequences in Table 2 can be run with TR < 6 s, including those proposed for lactate detection, and are therefore considered suitable for general application in quantitative studies.

8. In vivo performance

The SAR was monitored continuously to adhere to the current MDA guidelines. Healthy volunteers provided informed consent and the experimental protocol was approved by the University College London Hospital Ethics Committee. Fig. 11A shows an image slice from a structural Fast Spin-Echo (FSE) scan [45] with effective TE = 66 ms that was used to locate a 15 mm × 15 mm × 15 mm voxel in the thalamus of a healthy volunteer. Fig. 11B shows the corresponding spectrum obtained with L-FOCI at TE = 48 ms after a 12.8 min acquisition. Spectral post processing included eddy current correction [46], apodization with a 3 Hz exponential filter, and zero order phase correction only.

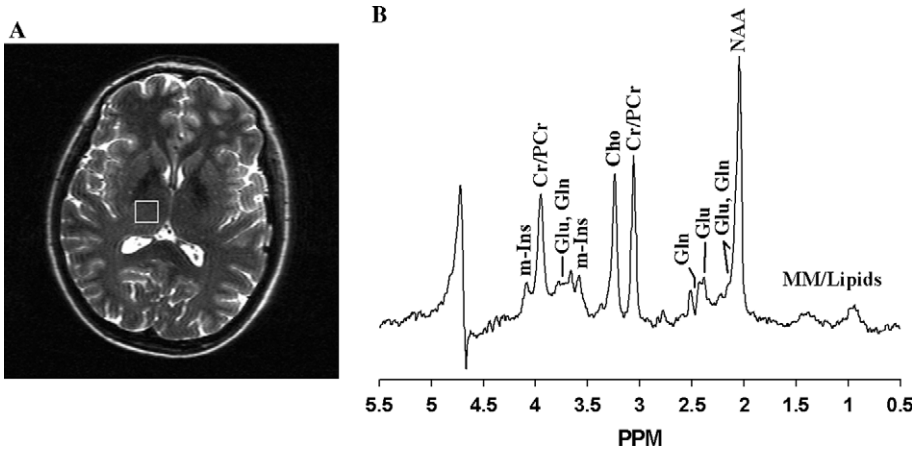

Fig. 11. (A) 4.7 T Fast Spin-Echo (FSE) image with effective TE = 66 ms. FOV = 20 cm × 20 cm. Slice thickness = 2 mm. The image shows a 15 mm × 15 mm × 15 mm voxel located in the thalamus of a healthy volunteer and centred at offsets $x = -15.1$ mm, $y = -21.4$ mm, and $z = 8.0$ mm with respect to the iso-centre of the head gradient set. (B) ^{1}H L-FOCI (LASER localisation using FOCI pulses) spectrum with TE = 48 ms from the voxel prescribed in (A). 128 scans were acquired with a 6 s repetition time in 12.8 min. NAA, *N*-acetylaspartate; Cr/PCr, creatine/phosphocreatine; Cho, choline containing compounds; m-Ins, *myo*-inositol; Glu, glutamate; Gln, glutamine; MM, macromolecules.

Water suppression was performed with VAPOR [47] in which the timings and flip angles were modified to accommodate 32 ms Gaussian suppression pulses without affecting VAPOR performance. The use of 32 ms Gaussian pulses ensures that signals below 4.2 ppm are not perturbed by the water suppression pulses. Shimming was performed by manual adjustment of *X*, *Y*, *Z*, and *Z*2 shim coils only. The creatine/phosphocreatine (Cr/PCr) singlet at 3.03 ppm exhibits a linewidth ($\Delta\nu_{1/2}$) of 11 Hz (including the 3 Hz of line broadening).

At a field strength of 1.5 T, it is generally accepted that glutamate (Glu) and glutamine (Gln) can not be distinguished, and a total value for Glx = Glu + Gln is the only meaningful measurement that can be made. The GAMMA calculations of individual metabolite resonances with 12 Hz line broadening show three peaks for Glu (2.07, 2.35, and 3.74 ppm) and three for Gln (2.11, 2.45, and 3.76 ppm). The calculated Glu and Gln peaks at 2.07 and 2.11 ppm, respectively, are largely obscured by the dominant *N*-acetylaspartate (NAA) singlet at 2.02 ppm, whilst those at 3.74 and 3.76 ppm, respectively, remain essentially indistinguishable at 4.7 T. It is, however, possible to tentatively assign the peak at 2.35 ppm to Glu, with no contribution from Gln, as the closest Gln signals are calculated to be offset by 20 Hz, at 2.45 ppm, corresponding to the trough indicated in Fig. 11B. The spectrum in this region is clearly complicated by the overlap of additional resonances and we anticipate that peak fitting methods such as LCModel will enable a more detailed and rigorous analysis of spectra. It is particularly encouraging to note that Glu and Gln have been consistently quantified individually, and with a reasonable degree of accuracy, following a spectral fitting analysis of human data acquired at 4 T [5].

9. Conclusions

It has been clearly demonstrated that significant improvements in spin-echo MRS at high field are possible when voxel localisation is performed using high BW FOCI pulses. At 4.7 T, FOCI pulses with BW = 20 kHz result in relatively small chemical shift displacement errors, extremely sharp and uniform selection profiles, and negligible contamination from outside of the voxel of interest. Given our current hardware limitations, single shot performance is only possible with TE $\geqslant$ 48 ms. It has been demonstrated that, for many metabolites at 4.7 T, localisation using FOCI pulses with TE = 48 ms results in ^{1}H anti-phase spectral components that are the same order as would be obtained from a symmetric PRESS sequence with TE = 32 ms. Furthermore, the T_2 losses should not be so severe because the six FOCI localisation pulses following initial excitation are expected to increase the apparent T_2 values of metabolite signals with respect to the two 180° pulses prescribed in PRESS. The small chemical shift displacement errors should enable good measurement of lactate using the TE = 144 and 288 ms timing schemes that have been proposed. Finally, even if significantly more RF power was available, it would be preferable, in terms of the SAR, to use relatively low power FOCI pulses rather than HS pulses with the same BW.

Acknowledgments

The authors thank The Wellcome Trust for providing the instrumentation and funding the work through Grant 045939/Z/95/Z. GAMMA is provided to the public courtesy of its authors. Detailed information and

platform downloading is available at http://gamma.magnet.fsu.edu.

References

[1] S. Posse, C.A. Cuenod, R. Risinger, D. Le Bihan, R.S. Balaban, Anomalous transverse relaxation in ^{1}H spectroscopy in human brain at 4 tesla, Magn. Reson. Med. 33 (1995) 246–252.

[2] G.F. Mason, G.M. Pohost, H.P. Hetherington, Numerically optimized experimental design for measurement of grey/white matter metabolite T_2 in high-resolution spectroscopic images of brain, J. Magn. Reson. B107 (1995) 68–73.

[3] S. Michaeli, M. Garwood, X.-H. Zhu, L. DelaBarre, P. Andersen, G. Adriany, H. Merkle, K. Uğurbil, W. Chen, Proton T_2 relaxation study of water, *N*-acetylaspartate, and creatine in human brain using Hahn and Carr–Purcell spin echoes at 4 T and 7 T, Magn. Reson. Med. 47 (2002) 629–633.

[4] R. Gruetter, S.A. Weisdorf, V. Rajanayagan, M. Terpstra, H. Merkle, C.L. Truwit, M. Garwood, S.L. Nyberg, K. Uğurbil, Resolution improvements in in vivo ^{1}H NMR spectra with increased magnetic field strength, J. Magn. Reson. 135 (1998) 260–264.

[5] R. Bartha, D.J. Drost, R.S. Menon, P.C. Williamson, Comparison of the quantification precision of human short echo time ^{1}H spectroscopy at 1.5 and 4.0 tesla, Magn. Reson. Med. 44 (2000) 185–192.

[6] I. Tkáč, P. Andersen, G. Adriany, H. Merkle, K. Uğurbil, R. Gruetter, In vivo ^{1}H NMR spectroscopy of the human brain at 7 T, Magn. Reson. Med. 46 (2001) 451–456.

[7] D. Hoult, Sensitivity and power deposition in a high-field imaging experiment, J. Magn. Reson. Imaging 12 (2000) 46–67.

[8] R.J. Ordidge, A. Connelly, J.A.B. Lohman, Image-selected in vivo spectroscopy (ISIS), J. Magn. Reson. 66 (1986) 283–298.

[9] R.E. Gordon, R.J. Ordidge, Volume selection for high resolution studies, in: Proceedings of the SMR, 3rd Annual Meeting, Berkeley, 1984, 272.

[10] P.A. Bottomley, Spatial localisation in NMR spectroscopy in vivo, Ann. N. Y. Acad. Sci. 508 (1987) 333–348.

[11] J. Frahm, K.-D. Merboldt, W. Hanicke, Localised proton spectroscopy using stimulated echoes, J. Magn. Reson. 72 (1987) 502–508.

[12] M. Garwood, L. DelaBarre, The return of the frequency sweep: designing adiabatic pulses for contemporary NMR, J. Magn. Reson. 153 (2001) 155–177.

[13] J. Slotboom, A.F. Mehlkopf, W.M.M.J. Bovée, A single-shot localization pulse sequence suited for coils with inhomogeneous RF fields using adiabatic slice-selective RF pulses, J. Magn. Reson. 95 (1991) 396–404.

[14] M.S. Silver, R.I. Joseph, D.I. Hoult, Highly selective $\pi/2$ and π pulse generation, J. Magn. Reson. 59 (1984) 347–351.

[15] M.N.E. Kassem, R. Bartha, Quantitative proton short-echo-time LASER spectroscopy of normal human white matter and hippocampus at 4 tesla incorporating macromolecule subtraction, Magn. Reson. Med. 49 (2003) 918–927.

[16] R.J. Ordidge, M. Wylezinska, J.W. Hugg, E. Butterworth, F. Franconi, Frequency offset corrected inversion (FOCI) pulses for use in localised spectroscopy, Magn. Reson. Med. 36 (1996) 562–566.

[17] S. Conolly, D. Nishimura, A. Macovski, G. Glover, Variable-rate selective excitation, J. Magn. Reson. 78 (1988) 440–458.

[18] G.B. Matson, FOCI pulses re-visited as re-mapped hyperbolic secant pulses, Proc. Intl. Soc. Magn. Reson. Med. 7 (1999) 2086.

[19] E.C. Wong, W.-M. Luh, Similarities and differences between FOCI pulses and VERSE transformed hyperbolic secant pulses, Proc. Intl. Soc. Magn. Reson. Med. 8 (2000) 1427.

[20] G.S. Payne, M.O. Leach, Implementation and evaluation of frequency offset corrected inversion (FOCI) pulses on a clinical MR system, Magn. Reson. Med. 38 (1997) 828–833.

[21] S. Conolly, G. Glover, D. Nishimura, A. Macovski, A reduced power selective adiabatic spin-echo pulse sequence, Magn. Reson. Med. 18 (1991) 28–38.

[22] L.N. Ryner, J.A. Sorenson, M.A. Thomas, 3D localized 2D NMR spectroscopy on an MRI scanner, J. Magn. Reson. B 107 (1995) 126–137.

[23] J.F. Bridges, Cavity resonator with improved magnetic field uniformity for high frequency operation and reduced dielectric heating in NMR imaging devices, US Patent 4751464 (1988).

[24] V. Govindaraju, K. Young, A.A. Maudsley, Proton NMR chemical shifts and coupling constants for brain metabolites, NMR Biomed. 13 (2000) 129–153.

[25] S.W. Provencher, Estimation of metabolite concentrations from localized in vivo proton NMR spectra, Magn. Reson. Med. 30 (1993) 672–679.

[26] S.W. Provencher, Automatic quantitation of localized in vivo ^{1}H spectra with LCModel, NMR Biomed. 14 (2001) 260–264.

[27] R.A. de Graaf, K. Nicolay, Adiabatic water suppression using frequency selective excitation, Magn. Reson. Med. 40 (1998) 690–696.

[28] M. Bunse, W.-I. Jung, O. Lutz, Localised double spin echo spectroscopy of weakly homonuclear coupled spin systems: influence of chemical shift artefacts, Appl. Magn. Reson. 3 (1992) 185–197.

[29] F. Schick, T. Nägele, U. Klose, O. Lutz, Lactate quantification by means of PRESS spectroscopy—influence of refocusing pulses and timing scheme, Magn. Reson. Imaging 13 (1995) 309–319.

[30] I. Marshall, J.M. Wild, Calculations and experimental studies of the lineshape of the lactate doublet in PRESS-localized ^{1}H MRS, Magn. Reson. Med. 38 (1997) 415–419.

[31] D.A. Yablonskiy, J.J. Neil, M.E. Raichle, J.J.H. Ackerman, Homonuclear *J* coupling effects in volume localized NMR spectroscopy: pitfalls and solutions, Magn. Reson. Med. 39 (1998) 169–178.

[32] I. Marshall, J.M. Wild, A systematic study of the lactate lineshape in PRESS-localized proton spectroscopy, Magn. Reson. Med. 40 (1998) 72–78.

[33] R.B. Thompson, P.S. Allen, Sources of variabilty in the response of coupled spins to the PRESS sequence and their potential impact on metabolite quantification, Magn. Reson. Med. 41 (1999) 1162–1169.

[34] W.-I. Jung, M. Bunse, O. Lutz, Quantitative evaluation of the lactate signal loss and its spatial dependence in PRESS localized ^{1}H NMR spectroscopy, J. Magn. Reson. 152 (2001).

[35] M. Garwood, Y. Ke, Symmetric pulses to induce arbitrary flip angles with compensation for RF inhomogeneity and resonance offsets, J. Magn. Reson. 94 (1991) 511–525.

[36] A. Tannús, M. Garwood, Improved performance of frequency-swept pulses using offset-independent adiabaticity, J. Magn. Reson. A120 (1996) 133–137.

[37] S.A. Smith, T.O. Levante, B.H. Meier, R.R. Ernst, Computer simulations in magnetic resonance. An object oriented programming approach, J. Magn. Reson. A106 (1994) 75–105.

[38] R.R. Ernst, G. Bodenhausen, A. Wokaun, Principles of Nuclear Magnetic Resonance in One and Two Dimensions, Clarendon Press, Oxford, 1987.

[39] E.B. Cady, J. Penrice, P.N. Amess, A. Lorek, M. Wylezinska, R.F. Aldridge, F. Franconi, J.S. Wyatt, E.O.R. Reynolds, Lactate, *N*-acetylaspartate, choline and creatine concentrations, and spin–spin relaxation in thalamic and occipito-parietal regions of developing human brain, Magn. Reson. Med. 36 (1996) 878–886.

[40] K.P. Whittall, A.L. MacKay, D.K.B. Li, Are mono-exponential fits to a few echoes sufficient to determine T_2 relaxation for in vivo human brain? Magn. Reson. Med. 41 (1999) 1255–1257.

[41] F. Träber, W. Block, R. Lamerichs, J. Gieseke, H.H. Schild, ^{1}H metabolite relaxation times at 3.0 tesla: measurements of T1 and T2 values in normal brain and determination of regional differences in transverse relaxation, J. Magn. Reson. Imaging 19 (2004) 537–545.
[42] Medical Devices Agency, in: Guidelines for magnetic resonance equipment in clinical use, United Kingdom Department of Health, MDA, 2002.
[43] T.S. Ibrahim, R. Lee, B.A. Baertlein, A. Kangarlu, P.-M.L. Robitaille, Application of finite difference time domain method for the design of birdcage RF head coils using multi-port excitations, Magn. Reson. Imaging 18 (2000) 733–742.
[44] T. Ethofer, I. Madar, U. Seeger, G. Helms, M. Erb, W. Grodd, A. Ludolph, U. Klose, Comparison of longitudinal metabolite relaxation times in different regions of the human brain at 1.5 and 3 tesla, Magn. Reson. Med. 50 (2003) 1296–1301.
[45] D.L. Thomas, E. De Vita, S. Roberts, R. Turner, T.A. Yousry, R.J. Ordidge, High-resolution fast spin echo imaging of the human brain at 4.7 T: implementation and sequence characteristics, Magn. Reson. Med. 51 (2004) 1254–1264.
[46] R.J. Ordidge, I.D. Cresshull, The correction of transient B_0 field shifts following the application of pulsed gradients by phase correction in the time domain, J. Magn. Reson. 69 (1986) 151–155.
[47] I. Tkáč, Z. Starčuk, I.-Y. Choi, R. Gruetter, In vivo ^{1}H NMR spectroscopy of rat brain at 1 ms echo time, Magn. Reson. Med. 41 (1991) 649–656.